Global Environmental Science
www.sciltp.com/journals/ges

Article

Microbial Community Dynamics in the Surface Water-Groundwater Interaction Zone of the Upper Miyun Reservoir Basin

Zhaoxin Li [1,2], Wenzhi Zhang [1,3], Junxiong Huang [1,*], Zhaoyong Bian [2,*], Lei Li [1], Wanlai Xue [1] and Wei Xiu [3,*]

1 Beijing Water Science and Technology Institute, Beijing 100048, China
2 College of Water Sciences, Beijing Normal University, Beijing 100875, China
3 State Key Laboratory of Biogeology and Environmental Geology, China University of Geosciences Beijing, Beijing 100083, China
* Correspondence: hjx@bwsti.com (J.H.); bian@bnu.edu.cn (Z.B.); xwsuron@cugb.edu.cn (W.X.)

How To Cite: Li, Z.; Zhang, W.; Huang, J.; et al. Microbial Community Dynamics in the Surface Water-Groundwater Interaction Zone of the Upper Miyun Reservoir Basin. *Glob. Environ. Sci.* **2026**, *2*(1), 23–37. https://doi.org/10.53941/ges.2026.100002

Publication History

Received: 4 November 2025
Revised: 9 December 2025
Accepted: 16 December 2025
Published: 22 December 2025

Keywords

surface water-groundwater interface;
nitrogen cycling;
microbial community;
environmental determinants;
community assembly processes

Highlights

- Frequent surface-water-groundwater interactions across the watershed basin
- Microbial nitrogen cycling roadmap indicating N-transformation hotspots
- Temperature, DO, and pH as key modulators of microbial co-occurrence networks

Abstract: Nitrogen (N) fluxes delivered from river inflows to reservoirs are critical for regulating nutrient dynamics and sustaining water quality in drinking-water source regions. In this study, we investigated the surface-water-groundwater interaction zone within the Chao-Bai River catchment, the primary inflow area feeding the Miyun Reservoir, which is the main water supply for Beijing. Our objective was to characterize the spatiotemporal variability of N species, microbial community compositions, assembly processes, and functional taxa, and to clarify their respective contributions to N cycling. Nitrate-N, which represented 88 ± 9% of total N, was consistently higher in the Chao River (wet season: 13.7 ± 12.6 mg/L; dry season: 11.5 ± 3.8 mg/L) than in the Bai River (wet season: 6.9 ± 5.0 mg/L; dry season: 7.0 ± 4.2 mg/L). Microbial assemblies differed markedly across hydrological compartments and seasons. During the wet season, *Novosphingobium* dominated surface waters, whereas *Limnohabitans* and *unclassified_Xanthobacteraceae* were prevalent in groundwater, and *Flavobacterium* was abundant in sediments. In the dry season, surface waters were co-dominated by *Flavobacterium* and *Limnohabitans*, while *Limnohabitans*, *Acidovorax*, and *Hydrogenophaga* were characteristic of groundwater communities. Temperature, dissolved oxygen, and pH emerged as the principal environmental drivers structuring microbial interactions. Stochastic processes primarily governed microbial community assembly in surface waters and sediments, whereas deterministic selection exerted stronger control in groundwater. Overall, the results demonstrate that hydrological connectivity and microbial dynamics interactively regulate N fluxes and transformation pathways at the river-reservoir interface. These insights provide a mechanistic foundation for improving nutrient management and protecting drinking-water sources in reservoir ecosystems.

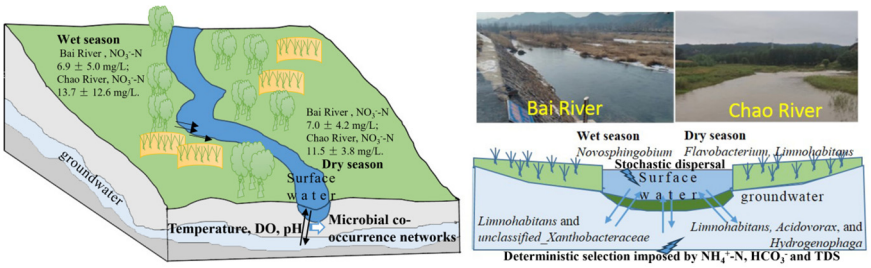

1. Introduction

Accelerating socioeconomic development and population growth have intensified nitrogen (N) pollution in freshwater systems, making excessive N loading a global environmental challenge. Elevated N inputs drive eutrophication, harmful algal blooms, and biodiversity loss in surface waters. In agroecosystems, the widespread application of synthetic fertilizers, combined with atmospheric deposition from fossil fuel combustion, continuously introduces reactive N into the environment, disrupting ecosystem structure and function [1]. In China, nearly 100,000 reservoirs form essential components of inland aquatic ecosystems, providing critical services such as water supply, hydropower generation, and irrigation [2]. National monitoring data from 204 major lakes and reservoirs indicate that approximately 90% experience some degree of eutrophication [3]. N enters aquatic systems predominantly in the form of nitrate (NO_3^-), which undergoes complex biogeochemical transformations and exchanges among the atmosphere, soils, waters, and biota [4]. Because most reservoirs are formed by damming rivers, the hydrochemical characteristics of tributary inflows play a decisive role in shaping reservoir ecological conditions. Consequently, increasing attention has been directed toward understanding and mitigating N pollution within tributary catchments.

Although extensive research has examined N dynamics in open surface waters, agricultural activities remain the dominant source of N inputs in high-yield catchments [1]. This pattern suggests that a large proportion of applied fertilizer N is not assimilated by crops but is instead lost from fields, generating environmental impacts that extend from local ecosystems to global biogeochemical cycles [5]. N concentrations in main-stem rivers are further amplified by inputs from tributaries; for instance, NO_3^- levels in the Yangtze River increase progressively downstream as tributaries contribute additional loads [6]. Despite this, current N-pollution control strategies remain largely centered on surface waters, overlooking the critical role of hydrologically dynamic exchange zones where surface water, groundwater, and sediments interact. Achieving a comprehensive understanding of N fate and transport, therefore, requires an integrated framework that explicitly incorporates the coupled processes operating across these interconnected compartments.

N, an essential element for all living organisms and the primary limiting nutrient in many ecosystems, occurs in several biologically active forms, including ammonium, nitrite, and nitrate, whose transformations are mediated by microbial biogeochemical processes [3,7]. Key pathways include N_2 fixation, nitrification, denitrification, anaerobic ammonium oxidation (anammox), assimilatory nitrate reduction to ammonium, and dissimilatory nitrate reduction to ammonium [8]. Recent discoveries, such as ammonia-oxidizing archaea, complete ammonia oxidizers (comammox *Nitrospira*), and atypical N_2O-reducing microbes, have reshaped our understanding of the global N cycle while simultaneously revealing its increasing complexity [7,9–11]. Although individual microbial taxa often exhibit low transformation efficiencies under fluctuating environmental conditions, the collective activity of diverse microbial communities can sustain substantially higher rates of N processing. This emphasizes the importance of examining community-level interactions rather than focusing solely on single organisms when evaluating N cycling [7]. Such microbial dynamics are especially critical in hydrologically active systems, where interactions among surface water, sediments, and groundwater jointly regulate N transformation pathways. These complexities underscore the need for integrated, cross-compartment approaches to fully resolve N cycling in river-reservoir continuums.

The Miyun Reservoir serves as a critical drinking-water source for Beijing, underscoring the importance of understanding N dynamics within its catchment to maintain water quality and ecosystem integrity. Because N cycling in this system is governed by complex interactions among surface water, sediments, and groundwater, a comprehensive, cross-compartment analysis is essential. Accordingly, this study aims to: (i) characterize the spatiotemporal variations of N species within the Chao-Bai River catchment; (ii) elucidate the structure of microbial communities and the ecological mechanisms governing their assembly; and (iii) identify the core microbial taxa responsible for major N transformation pathways. By integrating these components, the research provides a mechanistic basis for catchment-scale N-pollution mitigation

 https://doi.org/10.53941/ges.2026.100002

and supports science-informed strategies for ecological restoration and source-water protection.

2. Materials and Methods

2.1. Regional Overview

The Miyun Reservoir, the primary drinking-water source for Beijing, is situated within the mountainous terrain of Miyun District. The catchment exhibits a pronounced topographic gradient from north to south and west to east, and is largely shaped by the mountainous landscapes of the Yanshan Range within the Hai River system [12]. Administratively, the basin spans both Beijing Municipality and Hebei Province. Two major tributaries supply the reservoir: (i) the Chao River (CR), which originates in Fengning County (Hebei Province) and enters the reservoir via Gubeikou after passing through Luanping County; and (ii) the Bai River (BR), which begins in Guyuan County (Hebei), flows through Chicheng County, Yanqing District, and Huairou District, and ultimately discharges into the reservoir at Daguan Bridge. Together, these tributaries drain an area of 15,788 km^2 [12].

In addition to these main rivers, numerous small and often ephemeral tributaries contribute to the reservoir system. These channels typically remain dry during winter and spring but convey substantial runoff during summer and autumn, exhibiting strong intra-annual variability characteristic of mountainous hydrological regimes. Groundwater recharge in the catchment is primarily governed by precipitation, surface-water infiltration, and irrigation return flows [13,14].

In recent years, nitrogen concentrations in the Miyun Reservoir steadily increased, signaling an increasing risk of eutrophication [15,16]. Both the Chao and BRs deliver elevated nitrogen loads that critically influence reservoir water quality [17]. Additionally, significant groundwater nitrogen contamination has been documented within the basin, with strong hydrologic connectivity between groundwater and surface water [14,18]. Consequently, groundwater nitrogen dynamics are considered alongside surface-water processes in this study.

2.2. Sampling Design and Sample Collection

Following the watershed-integrity principle, we established 26 paired surface-water, sediment, and groundwater monitoring stations along the CR and BR, extending from their headwaters to the reservoir inflow zone (Figure 1). Site selection was designed to encompass a representative range of geomorphic settings, gradients in hydrologic connectivity, and locations influenced by potential pollution inputs. Sampling campaigns were carried out during November–December 2023 (dry season) and August–September 2024 (wet season), thereby capturing one full hydrologic cycle.

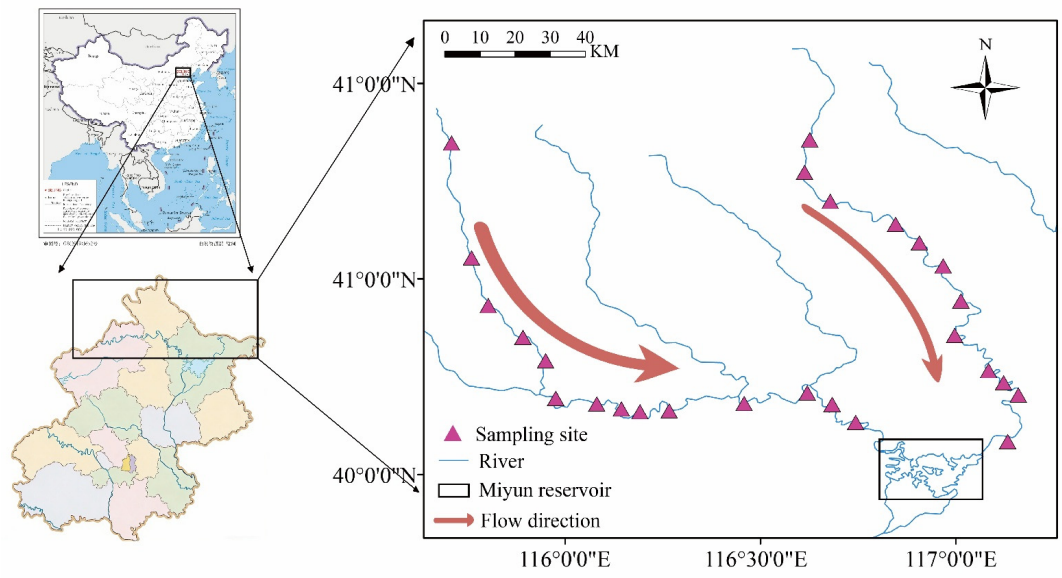

Figure 1. Spatial distribution of sampling sites.

At each sampling station, approximately 2.5 L of surface water was collected using a pre-sterilized acrylic sampler and transferred into sterile polyethylene containers. Surficial sediment (0–5 cm) was obtained with a stainless-steel grab sampler, homogenized on site, and subsampled into sterile 50 mL centrifuge tubes. For groundwater sampling, each well was purged for 25–30 min prior to collection while continuously monitoring temperature, pH, total dissolved solids (TDS), and oxidation-reduction potential using a calibrated multiparameter analyzer (YSI ProPlus, Yellow Springs, OH, USA). Groundwater was collected only after field parameters stabilized within ±5% across consecutive readings to ensure sample quality and representativeness. Following stabilization, approximately 15 L of groundwater was collected into acid-washed, sterile carboys for laboratory

analyses. For microbial analyses, 0.5–1 L of each water sample was filtered on site through 0.22 μm nitrocellulose membranes (Millipore, Darmstadt, Germany)). Filters were immediately snap-frozen on dry ice (−60 °C) and stored at −80 °C until DNA extraction and sequencing. For geochemical characterization, an additional 500 mL aliquot of water was filtered through 0.22 μm hydrophilic PVDF membranes into pre-acid-washed HDPE bottles (acidified to pH < 2 when required) and stored at 4 °C pending nutrient and trace-element analyses. For sediment samples, at least 20 g of homogenized material was aseptically transferred into sterile 50 mL tubes, snap-frozen (−60 °C), and archived at −80 °C for microbial assays. The remaining sediment was kept at 4 °C and processed within 48 h for physicochemical analyses.

2.3. Physicochemical Characterization

Surface-water temperature, pH, and dissolved oxygen (DO) were measured *in situ* using a calibrated multiparameter probe (YSI ProPlus, Yellow Springs, OH, USA) after instrument readings had stabilized. For groundwater, the same probe was deployed in the pumped-water stream during well purging to continuously monitor temperature, pH, and DO.

Concentrations of NO_3^--N, NO_2^--N, SO_4^{2-}, and other major ions were quantified by ion chromatography (ECO-IC, Metrohm, Herisau, Switzerland) following filtration through 0.22 μm membranes. Bicarbonate (HCO_3^-) was determined using a digital titrator (Model 16900, HACH) based on the bromocresol green-methyl red endpoint method. Stable isotopes δ^{15}N-NO_3^- and δ^{18}O-NO_3^- were analyzed via the denitrifier method coupled with isotope-ratio mass spectrometry [19].

2.4. DNA Extraction and Sequencing

Total genomic DNA was extracted from 0.22 μm membrane filters (water samples) and 0.5 g of wet sediment using the PowerWater® and PowerSoil® DNA Isolation Kits (MOBIO Laboratories, Carlsbad, CA, USA), respectively, following the manufacturers' protocols. DNA concentration and purity were evaluated using a NanoDrop™ One spectrophotometer and confirmed via agarose gel electrophoresis. To optimize amplification efficiency and minimize PCR cycle numbers, preliminary PCR assays were performed on randomly selected samples. PCR products exhibiting clear bands of the expected size and sufficient intensity on 2% agarose gels were selected for downstream processing. Extraction blanks and PCR negative controls were included throughout all procedures, with no detectable amplification observed, confirming the absence of contamination. For low-biomass groundwater samples, DNA yield was enhanced by filtering larger volumes (15 L), thereby improving reproducibility and downstream analysis quality.

PCR amplification targeted the V3-V4 hypervariable region of the 16S rRNA gene. Each 20 μL reaction contained 4 μL of 5× Fast Pfu Buffer, 2 μL of 2.5 mM dNTPs, 0.8 μL each of 5 μM primers 338F (5′-ACTCCTACG GGAGGCAGCAG-3′) and 806R (5′-GGACTACHVGGGTWTC TAAT-3′) [20], 0.4 μL Fast Pfu Polymerase, and 10 ng of template DNA. The thermal cycling protocol consisted of an initial denaturation at 95 °C for 3 min, followed by 30 cycles of 95 °C for 30 s, 58 °C for 30 s, and 72 °C for 45 s, with a final extension at 72 °C for 10 min. Equimolar amplicon libraries were subsequently prepared and sequenced on the Illumina MiSeq platform by Majorbio BioPharm Technology Co., Ltd. (Shanghai, China).

Quality control procedures involved removing reads with Phred scores below <Q20 and truncating forward and reverse reads to lengths of 270 bp and 260 bp, respectively. Paired-end reads were then merged to generate high-quality, full-length sequences. Chimeric sequences were identified and excluded, and exact amplicon sequence variants (ASVs) were inferred at 100% sequence similarity. Taxonomic classification of ASVs was performed using the naïve Bayes classifier implemented in QIIME 2 (sklearn) against the SILVA v138.2 database. To minimize contamination and sequencing artifacts, sequences identified as chloroplast, mitochondrial, or non-bacterial, as well as singletons (total frequency < 10 across all samples), were removed. The resulting ASV table was rarefied to the minimum sequencing depth across samples to standardize sampling effort before downstream ecological analyses.

2.5. Statistical Analysis

All statistical analyses were performed using R version 4.4.2. Pairwise comparisons were conducted using the Wilcoxon rank-sum test and visualized with the *ggplot2* package [21]. Multiple comparisons were assessed via the least-significant-difference test, implemented through the *ggsignif* [22] and *agricolae* [23] packages. Spearman's rank correlation was used to evaluate associations, with p-values adjusted for multiple testing using the Benjamini-Hochberg procedure via the *Hmisc* package [24]. Microbial α- and β-diversity indices were calculated using *vegan* [25], and dimensionality reduction was performed through principal component analysis and non-metric multidimensional scaling (NMDS). The modified stochasticity ratio (MST) was calculated with the *NST* package [26]. Microbial association networks were constructed in *Gephi* version 0.10.1 [27], and their topological properties were characterized using *ggClusterNet* [28].

3. Results and Discussion

3.1. Spatio-Temporal Variations of N Species

Using monthly surface-water sampling data collected from 2023 to 2024, we examined longitudinal variations in total N (TN) and nitrate-N (NO_3^--N)

 https://doi.org/10.53941/ges.2026.100002

concentrations along the Chao River (CR) and Bai River (BR) (Figure 2). Both rivers exhibited a characteristic "rise-then-decline" pattern in TN and NO_3^--N levels. In the BR, concentrations were initially low, increased sharply downstream, with TN occasionally reaching or exceeding 15 mg/L, before gradually decreasing toward the river's lower reaches. In contrast, the CR showed a modest peak in TN and NO_3^--N immediately below the headwaters, followed by a slow, continuous decline downstream. This downstream attenuation of N in both rivers suggests an intrinsic capacity for self-purification, likely driven by spatial shifts in microbial community composition along the flow path.

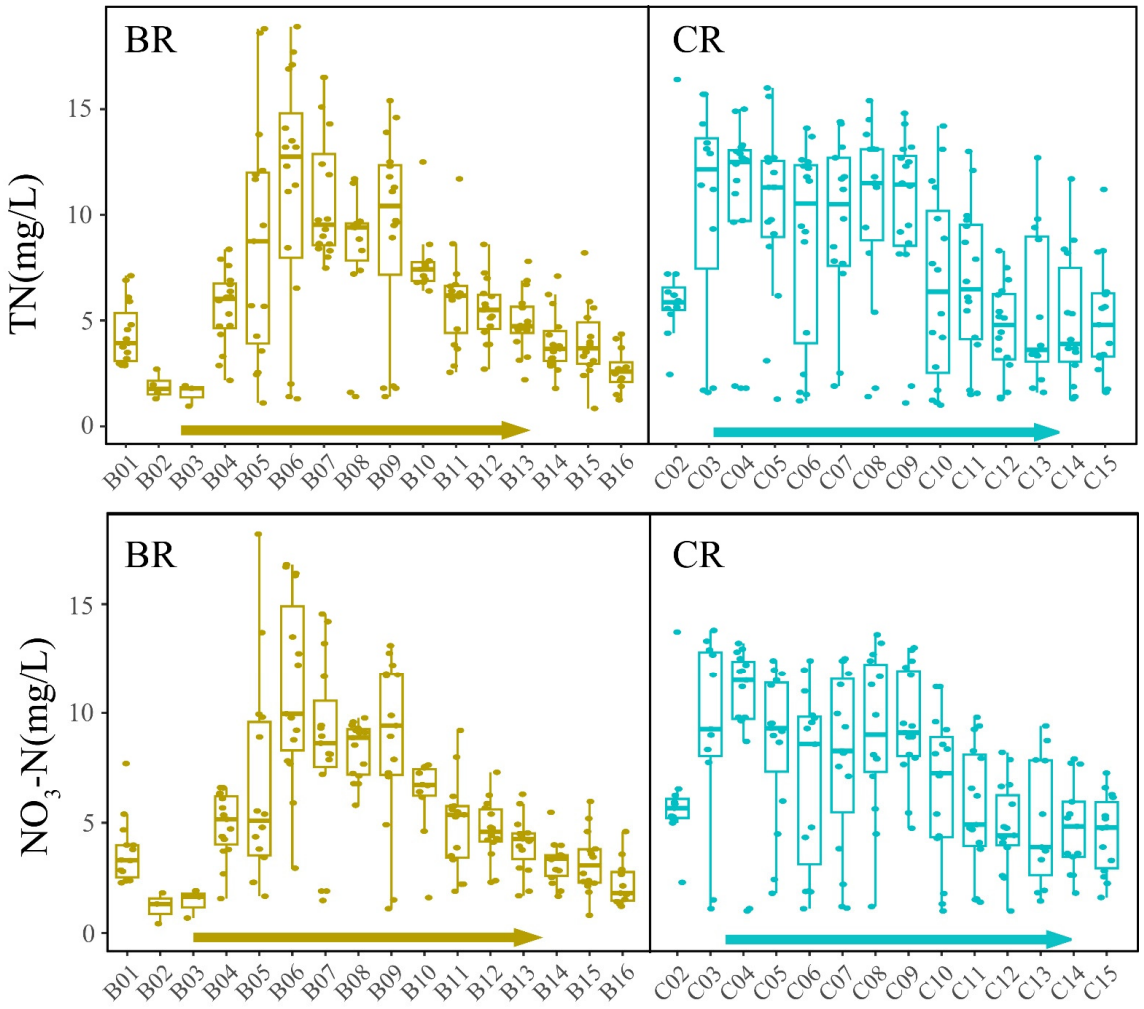

Figure 2. Longitudinal variations in surface-water TN and NO_3^--N concentrations in the Chao and Bai rivers, 2023–2024.

The synchronized longitudinal patterns observed in TN and NO_3^--N across the study area are primarily attributed to the dominant presence of NO_3^--N within the TN pool, which on average constitutes 88% ± 9% of total N.

The spatiotemporal distribution of NO_3^--N across the study area is illustrated in Figure 3. The overall mean NO_3^--N concentration across all samples was 9.3 ± 7.7 mg/L. Among surface-groundwater pairs, only the CR during the wet season exhibited significantly higher NO_3^--N levels in groundwater compared to surface water (Figure 3a,f); no significant differences were observed in other seasons or in the BR. Inter-basin comparisons revealed that the CR consistently carried significantly greater NO_3^--N loads than the BR during both wet (13.7 ± 12.6 mg/L vs. 6.9 ± 5.0 mg/L) and dry seasons (11.5 ± 3.8 mg/L vs. 7.0 ± 4.2 mg/L). This disparity is attributed to differing riparian land-use patterns: the CR corridor is dominated by intensive livestock and poultry operations, whereas the BR is primarily bordered by cropland. Compared to the diffuse leaching of fertilizers from agricultural fields, the accumulation of animal manure and its infiltration during rainfall events appear to be the primary drivers of elevated groundwater nitrate concentrations beneath the CR.

Longitudinal profiling revealed a consistent 'increase-then-decrease' pattern of NO_3^--N concentrations along both the Chao and BRs (Figure 3b–e,h–k). However, during the wet season, an anomalous groundwater peak was observed at site fC08 on the CR, where NO_3^--N concentrations spiked to 60 mg/L before declining sharply. This site is located adjacent to intensive livestock operations, and intense rainfall likely facilitated the rapid infiltration of manure-derived N, resulting in the observed groundwater nitrate surge.

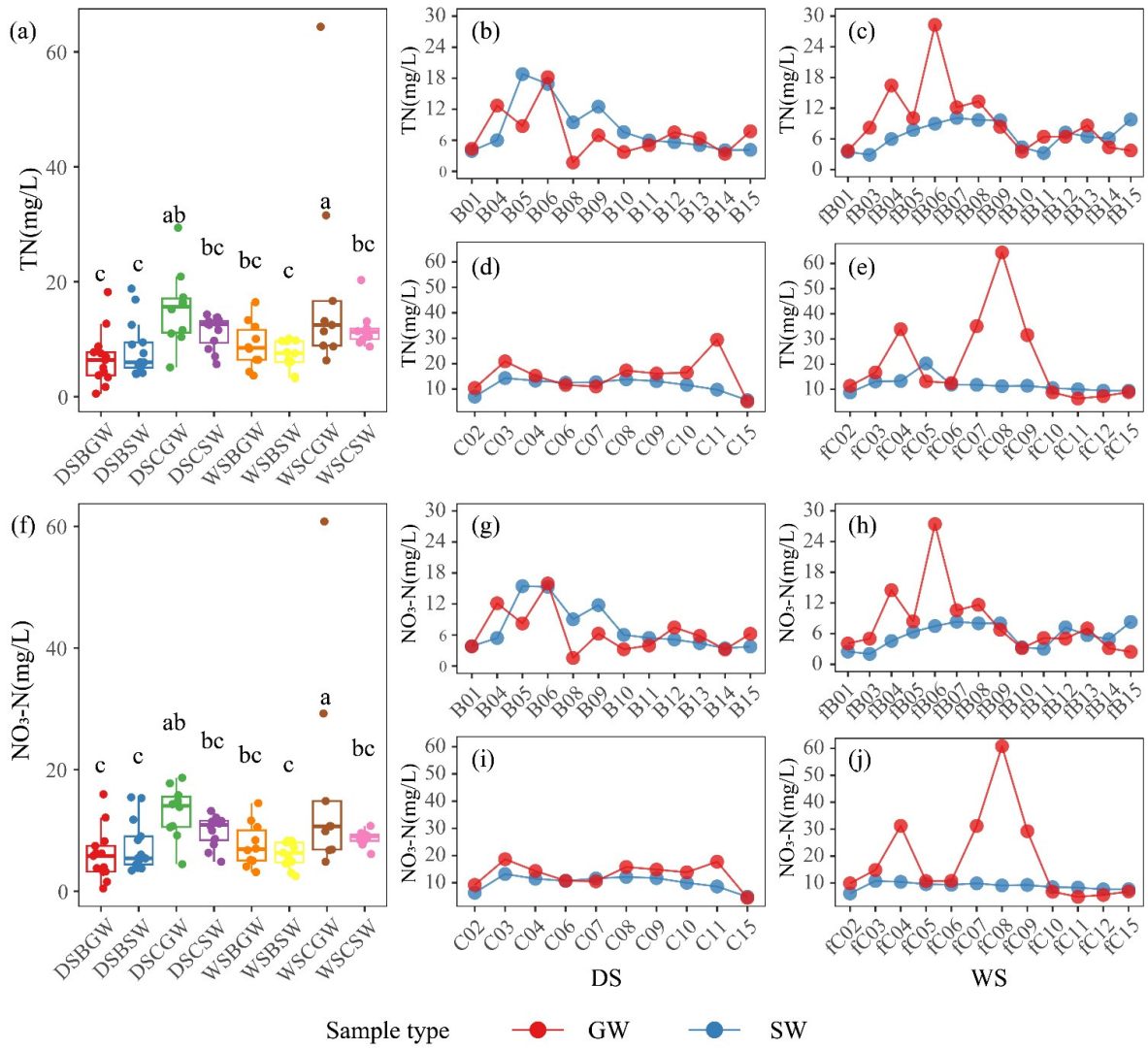

Figure 3. Variations in TN and NO_3^--N concentrations within the study area: (**a**,**f**) Boxplots of TN and NO_3^--N for different water-body types. (**b**–**e**, **g**–**j**) Longitudinal profiles of TN and NO_3^--N along the Chao and Bai rivers during dry and wet seasons, respectively.

In the upper BR, groundwater NO_3^--N concentrations were lower than those in surface water during the dry season, but this relationship reversed during the wet season, suggesting a shift in N sources and transport pathways across hydrological regimes. A similar inversion was observed in the lower CR, where surface-water NO_3^--N exceeded groundwater levels in the dry season, whereas groundwater concentrations were higher during the wet season. These hydrological reversals indicate that rainfall not only introduces additional N but also influences the direction and intensity of surface-water-groundwater exchange. Further downstream in the BR, NO_3^--N concentrations alternated between surface water and groundwater along the flow path, reflecting a dynamic and bidirectional recharge relationship. Overall, the spatiotemporal distribution of N within the catchment is governed by the combined effects of land-use patterns, hydrological processes, and anthropogenic activities. Seasonal shifts between wet and dry flow regimes emerge as key drivers regulating N transport and transformation throughout the system.

Spearman rank correlations between surface-water and groundwater chemistry at each paired sampling site were calculated to assess the degree of synchronous variability. As illustrated in Supplementary Materials Figure S1, TN, NO_3^--N, δ^{15}N-NO_3^-, δ^{18}O-NO_3^-, TDS, HCO_3^-, fluoride, chloride, and sulfate (SO_4^{2-}) all exhibited significant positive correlations ($p < 0.05$) between surface water and groundwater compartments. These results indicate tightly coupled temporal fluctuations and provide strong evidence for intensive surface-water-groundwater interactions throughout the study area.

N cycling in natural environments is well recognized as being tightly regulated by microbial processes [3,7]. In hydrological settings characterized by intensive surface-water-groundwater interactions and pronounced spatiotemporal variations in N, the composition and functional potential of microbial communities, and their responses to changing N forms, are especially critical.

 https://doi.org/10.53941/ges.2026.100002

Understanding how microorganisms respond to seasonal N dynamics is essential for elucidating the biogeochemical mechanisms underlying N transformations within this hydrologically connected system. These considerations form the conceptual framework for the microbial community analyses presented in the following sections.

3.2. Bacterial Diversity Characteristics

High-throughput sequencing of the 16S rRNA gene generated 23,058,200 clean reads, which were resolved into 30,634 bacterial ASVs. Taxonomic classification assigned these ASVs to 54 phyla, 172 classes, 424 orders, 747 families, and 1665 genera. Following rarefaction to the minimum sequencing depth of 17,814 reads per sample, rarefaction curves approached clear asymptotes (Supplementary Materials Figure S2), indicating that the sequencing effort was sufficient to capture the full extent of bacterial diversity within the samples.

As shown in Figure 4, α-diversity varied significantly among habitats, with Shannon diversity highest in sediment, intermediate in surface water, and lowest in groundwater. During the wet season, Shannon diversity in surface water was significantly greater than in the dry season (Wilcoxon test, $p < 0.05$), while no seasonal differences were observed in sediment or groundwater ($p > 0.05$) (Figure 4a,b; Supplementary Materials Table S1). Richness followed a similar habitat-specific pattern, with elevated values in wet-season surface water, whereas sediment and groundwater richness peaked during the DS (Figure 4c,d). Simpson indices showed minimal variation across samples and were generally high, indicating communities with relatively even species distributions (Figure 4e,f).

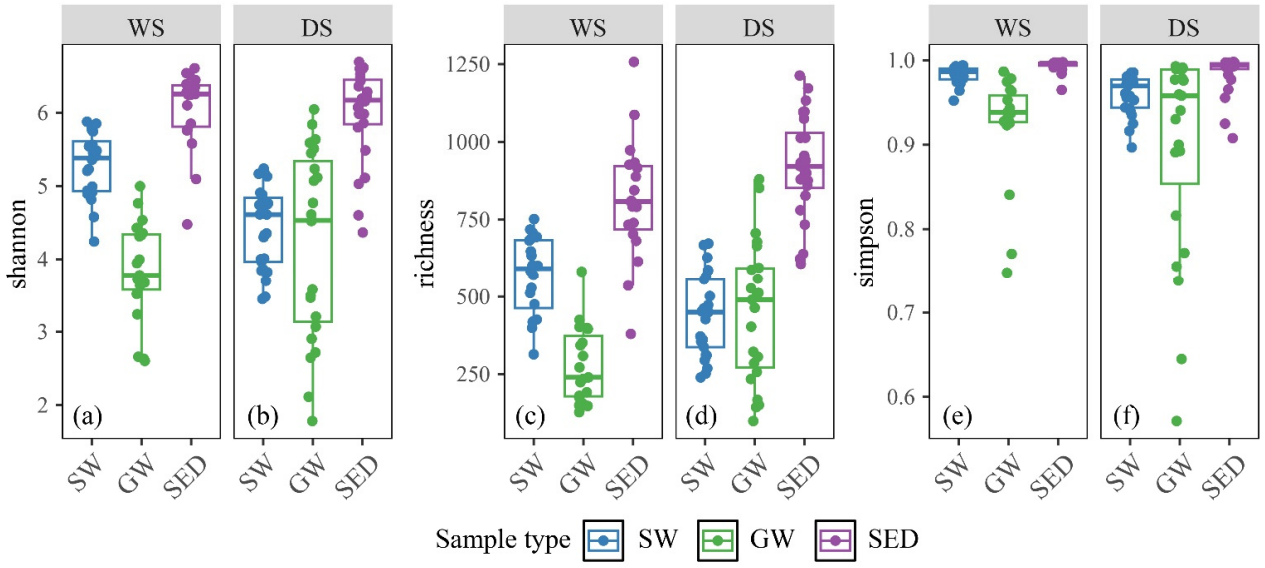

Figure 4. Comparisons of bacterial α-diversity among habitats: Box–whisker plots show Shannon (**a**,**b**), Richness (**c**,**d**) and Simpson (**e**,**f**) indices in surface water, sediment and groundwater during the wet season (left panels) and the dry season (right panels).

These observed patterns largely reflect hydrological forcing. Wet-season runoff and mixing introduce external microbes and nutrients, thereby enhancing surface-water diversity. In contrast, sediment and groundwater, being more buffered and stable environments, experience reduced disturbance, allowing species to accumulate during the dry season. This interpretation is further supported by coefficients of variation (Supplementary Materials Table S2), which reveal higher variability during the DS and greater homogenization in the wet season.

Hydrological processes largely explain these observed patterns. Wet-season rainfall enhances runoff and water-column mixing, introducing allochthonous microbes and nutrients that increase Shannon diversity, richness, and community evenness in surface water. In contrast, groundwater and sediment represent more buffered environments where reduced external forcing during the DS promotes species accumulation and higher richness. Although Simpson indices in groundwater and sediment remained generally stable across seasons, some dry-season groundwater samples exhibited slightly lower values, suggesting localized community unevenness that is alleviated by wet-season recharge. Sediment consistently supported the highest Shannon diversity, likely due to its heterogeneous microhabitats and greater nutrient availability, whereas the oligotrophic and hypoxic conditions in groundwater constrain microbial diversity [29]. Coefficients of variation [30] (Supplementary Materials Table S2) further corroborate this interpretation, showing higher variability during the DS and increased homogenization in the wet season. Overall, sediment hosted the greatest microbial diversity and richness, while groundwater exhibited the lowest values. This pattern reflects the complex mosaic of particle sizes,

organic-mineral interfaces, and redox gradients within sediment, which creates numerous ecological niches that promote species coexistence and reduce competitive exclusion [31,32]. The narrow range of Simpson indices indicates a consistently even community structure across samples. Hydrological forcing plays a critical role in shaping microbial diversity, most notably through wet-season amplification of surface-water richness, underscoring the importance of exogenous inputs and hydrodynamic processes in structuring microbial assemblages.

Analysis of microbial community composition across habitats and seasons (Supplementary Materials Figure S3) revealed significant differences among groups. During the wet season, *Novosphingobium* dominated surface waters, while *Limnohabitans* and unclassified *Xanthobacteraceae* prevailed in groundwater, and *Flavobacterium* typified sediments. In the dry season, surface-water communities shifted to a co-dominance of *Flavobacterium* and *Limnohabitans*, groundwater was characterized by *Limnohabitans*, *Acidovorax*, and *Hydrogenophaga*, whereas sediments maintained their *Flavobacterium* signature. β-diversity analysis using NMDS; Supplementary Materials Figure S4) demonstrated clear seasonal turnover in all habitats. Community composition differed significantly between wet (WS) and dry (DS) seasons in surface water ($R = 0.89$, $p < 0.001$), groundwater ($R = 0.30$, $p < 0.001$), and sediment ($R = 0.35$, $p < 0.001$). Wet-season samples clustered more tightly, indicating enhanced microbial dispersal under high-flow conditions. This pattern suggests that intense precipitation and increased hydrological connectivity homogenize environmental conditions and facilitate the dispersal of a shared microbial pool across surface water, groundwater, and sediment. Overall, hydrological connectivity emerges as a key driver shaping both α- and β-diversity across the studied habitats. This hydrologically mediated variability in microbial diversity and dispersal provides a critical foundation for understanding community assembly processes. In the following sections, we apply the neutral community model (NCM) and the normalized stochasticity ratio (MST) to quantify the relative contributions of stochastic dispersal and deterministic environmental filtering, thereby elucidating how N dynamics and hydrological regimes jointly influence microbial community structure in this coupled surface-water-groundwater system.

3.3. Assembly Processes Governing Microbial Community Formation

Microbial community assembly is commonly understood through two complementary theoretical frameworks: deterministic and stochastic processes. Deterministic processes, grounded in niche theory, are shaped by biotic interactions, such as competition, predation, symbiosis, and trade-offs, and abiotic filtering factors including salinity, pH, and temperature, which collectively constrain species distributions. In contrast, stochastic processes, based on neutral theory, assume ecological equivalence among species, with community structure emerging from random events such as births, deaths, dispersal, extinction, and speciation [33].

Two complementary frameworks, the NCM and the MST, were employed to quantify the relative contributions of stochastic and deterministic mechanisms governing microbial community assembly [34].

The NCM results (Figure 5) revealed distinct seasonal and habitat-specific patterns. During the WS, the goodness-of-fit (R^2) followed the order: sediment (0.67) > surface water (0.63) > groundwater (−0.22), while the migration rate (Nm) ranked similarly: sediment (251) > surface water (216) > groundwater (23). The negative R^2 value for groundwater indicates a significant deviation from neutral model expectations, suggesting strong environmental filtering or biotic interactions shaping community assembly. In contrast, sediment and surface water communities fit the neutral model well, implying that stochastic dispersal processes predominantly govern their assembly. During the DS, both R^2 and Nm values maintained the same hierarchical order but were generally lower than in the wet season, reflecting that hydrologic stability during the dry phase intensifies deterministic influences on microbial community assembly [35].

The MST quantifies the relative influence of deterministic versus stochastic forces in community assembly, ranging from 0 to 1, where higher values indicate a stronger role for stochastic processes [36]. The MST results (Supplementary Materials Figure S5) align closely with those from the NCM. During the WS, mean MST values (± SD) were highest in surface water (0.68 ± 0.23), followed by sediment (0.64 ± 0.23), and lowest in groundwater (0.56 ± 0.23). In the DS, MST values decreased across all habitats: surface water (0.53 ± 0.22), sediment (0.43 ± 0.21), and groundwater (0.28 ± 0.20). Wilcoxon tests confirmed that MST values were significantly higher in WS than in DS ($p < 0.001$) and differed significantly among habitats (Supplementary Materials Table S3). This seasonal pattern indicates that assembly processes follow the sequence: groundwater (most deterministic) < sediment (intermediate) < surface water (most stochastic). Hydrological forcing is the primary driver, with intense rainfall and increased runoff during the WS enhancing microbial dispersal and elevating stochasticity. Conversely, the stable, resource-limited conditions of the DS intensify niche-based selection, especially in groundwater, where low migration rates (Nm) reinforce deterministic assembly.

 https://doi.org/10.53941/ges.2026.100002

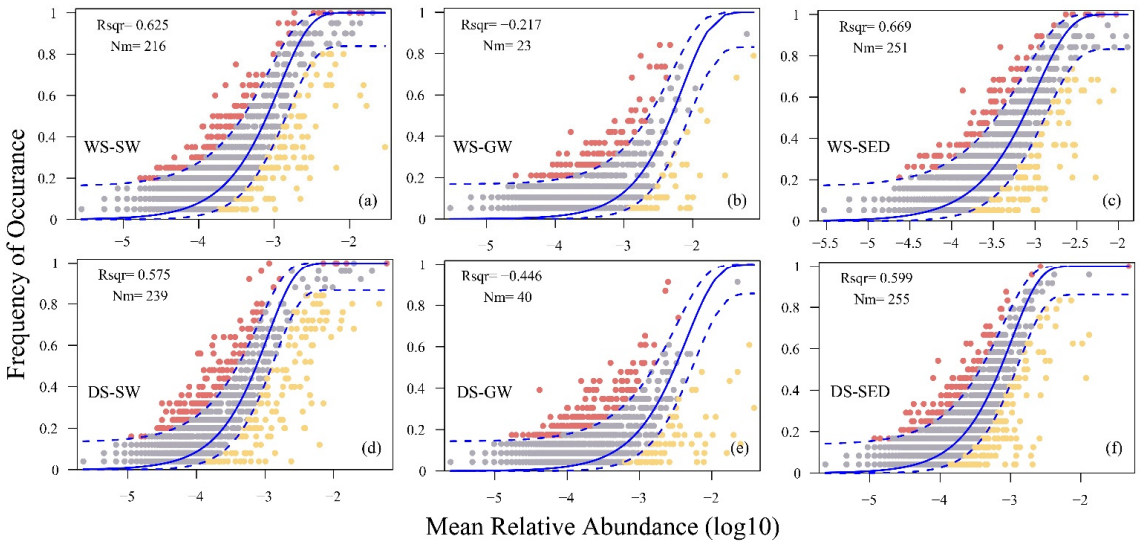

Figure 5. Neutral Community Model (NCM) fits for surface water (**a**,**d**), groundwater (**b**,**e**), and sediment (**c**,**f**) during the wet season (WS; **a**–**c**) and the dry season (DS; **d**–**f**).

To identify environmental drivers shaping microbial community assembly across habitats and seasons, we conducted linear regression analyses between the absolute differences in environmental variables and the MST index (Figure 6). The results reveal that community assembly is influenced by distinct factors depending on habitat and season, underscoring pronounced spatiotemporal heterogeneity in microbial structuring.

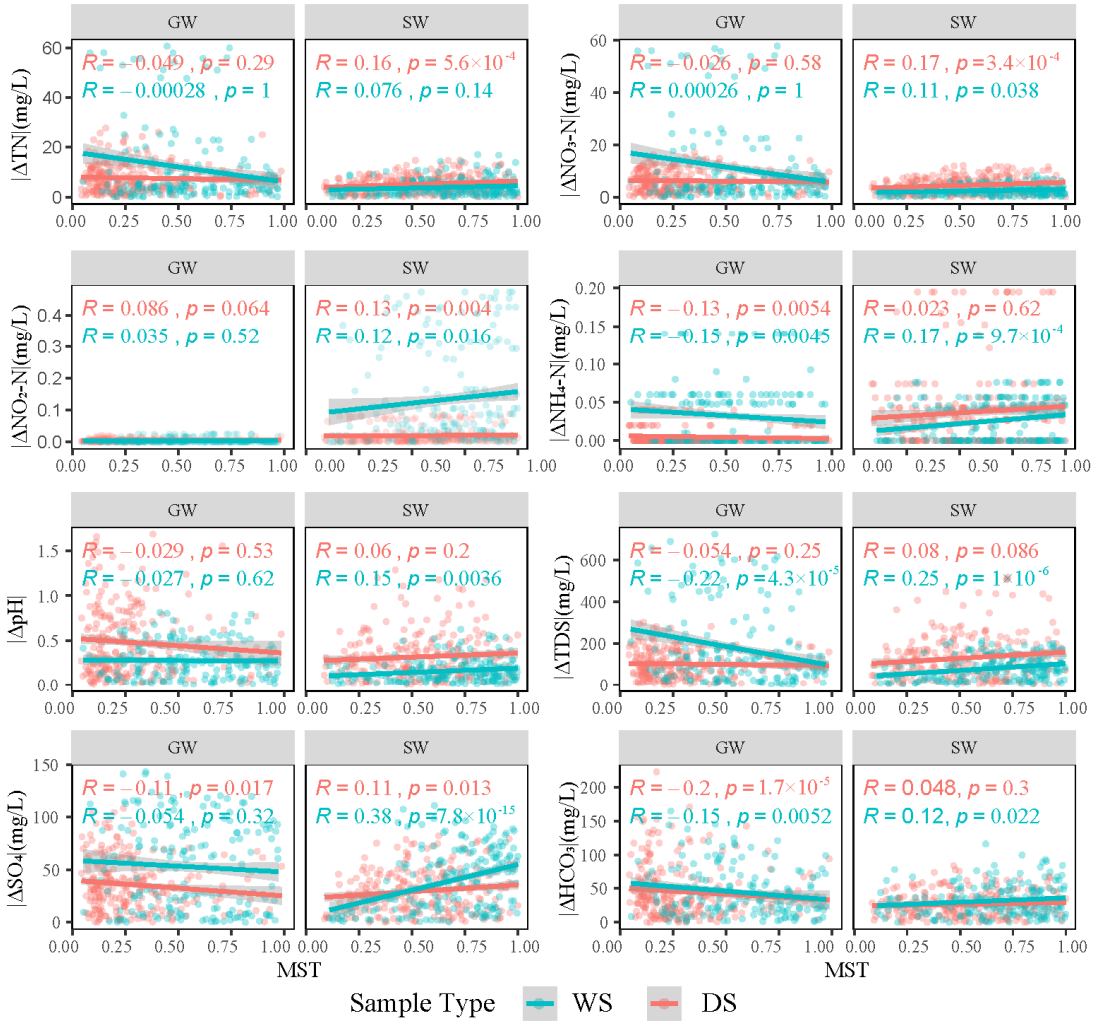

Figure 6. Linear regression between the absolute differences in environmental factors and the MST index.

In groundwater, community assembly was primarily driven by ammonium N (NH_4^+-N), HCO_3^-, and TDS ($p < 0.05$), suggesting that N availability and overall ionic strength strongly regulate microbial interactions within this relatively buffered environment. In surface water, assembly was influenced by nitrate (NO_3^--N), nitrite (NO_2^--N), ammonium (NH_4^+-N), pH, TDS, $SO4^{2-}$, and (HCO_3^-). Among these, NH_4^+-N, pH, TDS, and HCO_3^- exerted the strongest effects during the wet season, reflecting the impact of increased nutrient inputs and hydrological mixing, while the other factors influenced assembly across both seasons. These findings indicate that surface-water microbial communities are shaped by a combination of nutrient availability, chemical conditions, and seasonal hydrological fluctuations, whereas groundwater communities are primarily governed by a narrower suite of physicochemical parameters.

Given the central role of N in shaping microbial ecology, we further investigated the distribution and potential interactions of N-cycling microorganisms. To this end, microbial network analysis was performed to identify co-occurrence patterns and potential functional linkages. This approach provides mechanistic insights into how environmental drivers, especially N species, influence community assembly and interspecies interactions across surface water, groundwater, and sediment habitats.

3.4. Co-Occurrence Network Characteristics

N-cycling microorganisms were consistently abundant across habitats and seasons (Supplementary Materials Figure S3). In wet-season surface water, *Novosphingobium*, widely distributed in aquatic and terrestrial environments [37], is capable of reducing nitrate to nitrite, thereby contributing to denitrification and water self-purification [38,39]. *Sphingorhabdus* (wet-season surface water) was assoclated nitrite oxidation [40]. *Unclassified Xanthobacteraceae* (wet-season groundwater) are known diazotrophs that convert atmospheric N_2 to NH_4^+ under low-N conditions [41]. *Pseudomonas* (dry-season surface water) is an efficient N-fixing genus that enhances bioavailable N in oligotrophic waters [42]. In groundwater, both seasons saw *Acidovorax* and *Hydrogenophaga*, with *Acidovorax* involved in nitrification and denitrification [43], while *Hydrogenophaga* utilizes H_2 as an electron donor for heterotrophic denitrification, facilitating N removal [44]. *Limnohabitans* and *Acinetobacter* (wet-season surface water and groundwater) also play key roles: *Limnohabitans* exhibits ammonia-oxidizing potential [45], whereas *Acinetobacter* mediates heterotrophic nitrification-aerobic denitrification [46]. Finally, *Flavobacterium*, dominant in wet-season sediment and dry-season surface water, includes diazotrophic species [47] and contributes to denitrification pathways [39].

To elucidate potential ecological interactions, co-occurrence networks were constructed separately for the wet and dry seasons. Only ASVs present in at least 20% of samples were retained, and network edges were inferred using random matrix theory. Comparison with Erdős-Rényi random graphs [48] revealed significant structural deviations (Supplementary Materials Figure S6), confirming that the inferred networks reflect genuine ecological relationships rather than stochastic patterns.

Network-level analyses revealed pronounced seasonal restructuring of microbial interactions (Figure 7). The WS network comprised 431 nodes, while the DS network had 300 nodes. Only 109 ASVs were shared between seasons, with 322 and 191 ASVs unique to WS and DS, respectively, indicating distinct seasonal turnover in co-occurrence patterns. Regarding node degree, over 70% of ASVs exhibited degrees greater than 10 in both seasons (WS: 77.0%, DS: 72.3%), reflecting densely connected communities. However, WS networks had significantly higher degrees overall (Wilcoxon test, $p < 0.05$; Supplementary Materials Figure S7a). Notably, 16.5% of WS nodes exceeded a degree of 100, whereas no DS node reached this threshold (Supplementary Materials Figure S7b,c).

Network connectance, a measure of the density of microbial interaction networks [49], was quantified for each sample and correlated with environmental physicochemical variables to identify drivers of network architecture. As shown in Supplementary Materials Figure S8, temperature (T), DO, and pH significantly influenced connectance across both hydrological seasons (Supplementary Materials Figure S8a–c).

During the dry season, temperature exhibited a significant negative correlation with connectance ($p < 0.05$), indicating that elevated temperatures reduced network density. This inverse relationship likely reflects the dominance of psychrotolerant taxa adapted to low temperatures; warming diminishes their competitive advantage, thereby weakening inter-taxa interactions. In contrast, during the wet season, temperature correlated positively with connectance ($p < 0.05$), suggesting that higher temperatures stimulate microbial metabolism and strengthen network connectivity.

DO and pH were positively associated with connectance in both seasons ($p < 0.05$), although the effect of DO was notably stronger during the dry season. This pronounced influence of DO under low-flow conditions is attributed to spatial heterogeneity in oxygen availability, which critically constrains microbial interactions. Enhanced water-column mixing during the WS homogenizes DO concentrations, reducing, but not eliminating, its regulatory impact. The sustained positive correlation with pH suggests that moderate alkalinity promotes interspecific interactions, although this effect is likely threshold-dependent, with further pH increases beyond a certain point no longer enhancing connectance.

 https://doi.org/10.53941/ges.2026.100002

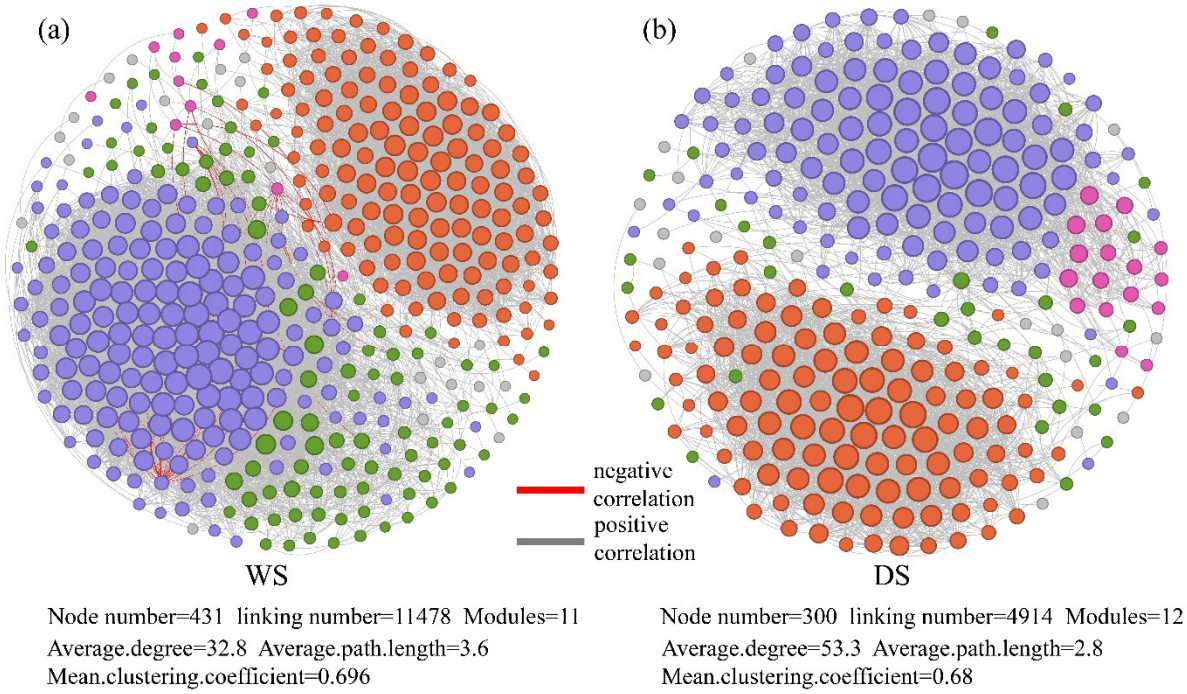

Figure 7. Microbial co-occurrence networks based on Random Matrix Theory (RMT): (**a**) Wet-season network (WS); (**b**) Dry-season network (DS).

Further analysis revealed that HCO_3^-, nitrite-N (NO_2^--N), and $SO4^{2-}$ influenced network connectance exclusively during the WS (Supplementary Materials Figure S8d,f,h). Both HCO_3^- and $SO4^{2-}$ exhibited significant negative correlations with connectance, suggesting that elevated concentrations of these ions suppress microbial interactions and reduce network density. In contrast, NO_2^--N showed a significant positive relationship with connectance, indicating that moderate increases in nitrite may promote the growth and cross-feeding of specific taxa, thereby strengthening microbial linkages [50]. Notably, these ion-driven effects were only apparent under high-flow conditions. Consistent with the hydrochemical profile of the study area, concentrations of all three anions increased during the wet season; however, absolute NO_2^--N levels remained low, implying that even slight elevations are sufficient to enhance network connectivity. During the wet season, nitrate concentration and its $\delta^{15}N$ isotopic signature were negatively correlated with microbial network connectance, whereas in the DS only $\delta^{15}N$ exhibited a weak positive association. Overall, these nitrate-related variables exerted only marginal influence on network connectance, likely because consistently high ambient nitrate concentrations limit its role as a controlling factor within the system.

Collectively, temperature, DO, and pH emerge as the key master variables shaping microbial network architecture across hydrological phases. Temperature exerts contrasting effects between seasons, negatively impacting network connectance during the DS but enhancing it in the wet season. DO limitation has the strongest influence under low-flow conditions, while pH consistently promotes microbial interactions regardless of season. Additionally, certain solutes, HCO_3^-, NO_2^--N, and SO_4^{2-}, modulate network connectivity exclusively during the wet season, highlighting the crucial role of dynamic hydrological shifts in reconfiguring microbial association networks.

The degree-betweenness plot (Figure 8) further revealed distinct topological roles among microbial taxa [51]. Taxa exhibiting high degree but low betweenness functioned primarily as keystone taxa within individual modules, indicating strong connectivity within their own modules rather than influence across multiple modules.

During the dry season, *Hydrogenophaga, MND1*, *Rhizobiales*, and *unclassified Hyphomicrobiaceae* exhibited high degree but low betweenness, underscoring their roles as core taxa within module-level substructures. *Hydrogenophaga*, ranking among the top ten most abundant genera in groundwater, is known to utilize H_2 as an electron donor to support heterotrophic denitrification [52]. Members of *Hyphomicrobiaceae* can exploit N_2, NO_3^-, or NH_3 as N sources and harbor nitrate- and nitrite-reductase genes, enabling complete denitrification to N_2 [53]. *MND1* has been associated with ammonia-oxidizing functions [54], while *Rhizobiales* includes well-documented diazotrophic lineages capable of N fixation [55]. These functional profiles indicate that N-transforming microorganisms dominate module-level structural roles under low-flow, resource-limited conditions.

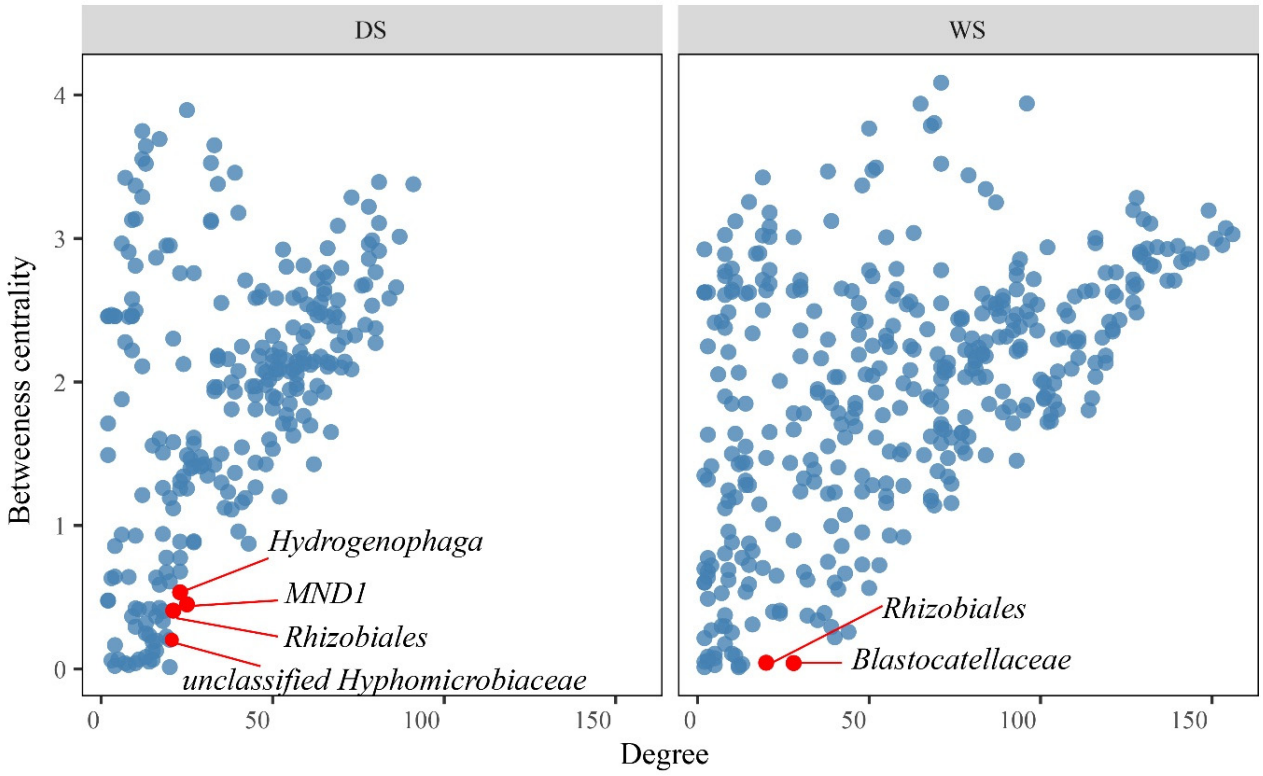

Figure 8. Degree–betweenness plot showing the distinct topological roles of microbial taxa.

In the wet season, *Rhizobiales* and *Blastocatellaceae* also exhibited high-degree but low-betweenness characteristics. The consistent role of *Rhizobiales* as a local hub across both seasons, coupled with its N-fixing capabilities, highlights the persistent importance of diazotrophs within microbial interaction modules. *Blastocatellaceae*, typically oligotrophic bacteria, are known for their efficiency in utilizing recalcitrant organic matter to sustain nutrient cycling, which likely contributes to their prominence during the hydrologically dynamic and nutrient-fluctuating conditions of the wet season.

Taken together, the keystone taxa identified across seasons were strongly enriched with N-cycling functional traits, including N fixation, nitrification, denitrification, and ammonium transformation, underscoring the central role of N biogeochemistry in structuring microbial interaction networks. These findings collectively demonstrate that biogeochemical functionality, particularly N cycling, is a defining characteristic of network keystones within this interconnected groundwater-surface-water system.

4. Conclusions

Nitrate constitutes 88 ± 9% of total N in the surface-groundwater continuum, with concentrations peaking mid-reach at 9.3 ± 7.7 mg/L NO_3^--N. Spatiotemporal N patterns are shaped by hydrology, land use, and anthropogenic inputs, with the transition from wet to dry seasons critically modulating N transport. 16S rRNA profiling reveals a declining α-diversity gradient, sediment > surface water > groundwater, while β-diversity reflects seasonal turnover driven by hydrological connectivity. Neutral and stochastic modeling shows groundwater microbial assemblages are deterministically structured by NH_4^+-N, HCO_3^-, and TDS, whereas surface communities are shaped predominantly by stochastic dispersal during the wet season. Co-occurrence networks expand substantially in the WS (431 nodes, 11,478 edges) compared to the DS (300 nodes, 4914 edges), anchored by N-cycling and sulfate-reducing taxa. Keystone modules, dominated by diazotrophs and denitrifiers, including *Rhizobiales, Hydrogenophaga, MND1*, *Hyphomicrobiaceae*, and *Blastocatellaceae*, exhibit high within-module connectivity but low inter-module betweenness, forming a resilient, N-focused guild that sustains nutrient cycling across hydrological extremes. Together, hydrological connectivity, habitat heterogeneity, and nutrient availability govern N mobility and microbial community assembly, providing a mechanistic blueprint for watershed-scale natural N-removal engineering.

Supplementary Materials

The additional data and information can be downloaded at: https://media.sciltp.com/articles/others/2512221534310595/GES-25110017-Supplementary-Materials.pdf. Figure S1: Spearman correlation of surface-water versus groundwater at the same sampling sites for (**a**) TN; (**b**) NO_3^--N; (**c**) $\delta^{15}N$-NO_3^-; (**d**) $\delta^{18}O$-NO_3^-; (**e**) TDS; (**f**) HCO_3^-; (**g**) F^-; (**h**) Cl^-; and (**i**) SO_4^{2-}. Figure S2: Rarefaction curves for wet-season samples (**a**) and dry-season samples (**b**). Figure S3: Relative abundance of the top bacterial genera across habitats and seasons: Stacked

 https://doi.org/10.53941/ges.2026.100002

bar charts display the ten most abundant genera at each site, (**a**) surface water—wet season; (**b**) groundwater—wet season; (**c**) sediment—wet season; (**d**) surface water—dry season; (**e**) groundwater—dry season; (**f**) sediment—dry season. Figure S4: Beta-diversity patterns of bacterial communities across habitats: Nonmetric multidimensional scaling (NMDS) ordinations within surface water (**a**); groundwater (**b**); and sediment (**c**) between the dry and wet seasons. Figure S5: Modified Stochasticity Ratio (MST) across habitats and seasons. Box-and-whisker plots show MST values (mean ± SD) for surface water (SW), groundwater (GW), and sediment (SED) during the wet (WS) and dry (DS) seasons. Figure S6: Comparison between the observed microbial community network and the E-R random network model. Figure S7: Differences in network node degree between wet-season and dry-season networks (**a**) and their degree distributions (**b**,**c**). The meanings represented by different asterisks. *** $p < 0.001$. Figure S8: Correlations between network connectance and physicochemical variables: the relationship between connectance and (**a**) temperature (T); (**b**) dissolved oxygen (DO); (**c**) pH; (**d**) bicarbonate (HCO_3^-); (**e**) nitrate-N (NO_3^--N); (**f**) nitrite-N (NO_2^--N); (**g**) $\delta^{15}N$-NO_3; (**h**) sulfate (SO_4^{2-}). Table S1: Results of Wilcoxon tests for differences in α-diversity indices among groups. Table S2: Coefficient of variation (CV) of α-diversity indices across different seasons and habitats. Table S3: Results of Wilcoxon tests for differences between different sample types.

Author Contributions

Z.L.: formal analysis, methodology, investigation, data curation, writing—original draft, resources; W.Z.: conceptualization, methodology, validation, visualization, software; J.H.: resources, investigation, supervision, writing—review; Z.B.: resources, supervision, writing—review; L.L.: investigation, data curation; W.X.: resources, investigation; W.X.: resources, writing editing. All authors have read and agreed to the published version of the manuscript.

Funding

This research was funded by Beijing Postdoctoral Research Foundation and Beijing Municipal Science and Technology Plan Project (Z221100005222013).

Institutional Review Board Statement

Not applicable.

Informed Consent Statement

Not applicable.

Data Availability Statement

Data will be made available on request.

Acknowledgments

The authors would like to express their thanks to the financial support from Beijing Postdoctoral Research Foundation.

Conflicts of Interest

The authors declare no conflict of interest.

Use of AI and AI-assisted Technologies

No AI tools were utilized for this paper.

References

1. Cai, Y.; Feng, M.; Zhang, T. Review of Distribution of Nitrogen and Phosphorus in Riparian Zones of Chinese Inland Water Bodies. *Acta Ecol. Sin.* **2022**, *42*, 583–592.
2. Sun, M.; Zhang, L.; Yang, R.; et al. Water Resource Dynamics and Protection Strategies for Inland Lakes: A Case Study of Hongjiannao Lake. *J. Environ. Manag.* **2024**, *355*, 120462.
3. Ning, H.; Jiang, W.; Sheng, Y.; et al. Comprehensive Evaluation of Nitrogen Contamination in Water Ecosystems of the Miyun Reservoir Watershed, Northern China: Distribution, Source Apportionment and Risk Assessment. *Environ. Geochem. Health* **2024**, *46*, 278.
4. Zhang, X.; Qi, Y.; Li, H.; et al. Assessing the Response of Non-Point Source Nitrogen Pollution to Land Use Change Based on SWAT Model. *Ecol. Indic.* **2024**, *158*, 111391.
5. Xu, W.; Cai, Y.; Rong, Q.; et al. Agricultural Non-Point Source Pollution Management in a Reservoir Watershed Based on Ecological Network Analysis of Soil Nitrogen Cycling. *Environ. Sci. Pollut. Res.* **2018**, *25*, 9071–9084.
6. Sarah, H.L.; Martin, B.; Robin, G.; et al. Connecting Diverse Disciplines to Improve Understanding of Surface Water-Groundwater Interactions. *J. Hydrol. X* **2022**, *17*, 100141.
7. Ren, Y.; Xu, Z.; Zhang, X.; et al. Nitrogen Pollution and Source Identification of Urban Ecosystem Surface Water in Beijing. *Front. Environ. Sci. Eng.* **2014**, *8*, 106–116.
8. Andrew, C.P.; Richard, I.; Stuart, B.; et al. Source Partitioning Using Stable Isotopes: Coping with Too Much Variation. *PLoS ONE* **2010**, *5*, e9672.
9. Stein, L.Y.; Klotz, M.G. The Nitrogen Cycle. *Curr. Biol.* **2016**, *26*, R94–R98.
10. Cao, Q.; Wang, H.; Chen, X.; et al. Composition and Distribution of Microbial Communities in Natural River Wetlands and Corresponding Constructed Wetlands. *Ecol. Eng.* **2017**, *98*, 40–48.
11. Stonedahl, S.H.; Sawyer, A.H.; Stonedahl, F.; et al. Effect of Heterogeneous Sediment Distributions on Hyporheic Flow in Physical and Numerical Models. *Groundwater* **2018**, *56*, 934–946.
12. Cheng, B.; Jiang, B.; Zhang, R.; et al. Variation Analysis of Long-term TN Concentration and Influencing Factors in Miyun Reservoir in China. *Glob. NEST J.* **2023**, *25*, 138–147.
13. Bao, Y.; Zhang, D.; Wang, Y.; et al. Analysis of Nitrogen Migration and Transformation in the Typical Deep and Large Reservoir of the Lancang River—Evidence from Nitrogen and Oxygen Isotopes. *J. Hydrol.* **2024**, *640*, 131701.
14. He, D.; Xie, X.; Liu, T.; et al. Fast Migrations of Nitrogen and Phosphorus Are Driven by Microorganism in Freshwater Lake Sediments. *J. Soils Sediments* **2024**, *24*, 1391–1401.

15. He, Z.; Cai, J.; Ni, Z.; et al. Seasonal Characteristics of Nitrogen Sources from Different Ways and Its Contribution to Water Nitrogen in Lake Erhai. *Acta Sci. Circumstantiae* **2018**, *38*, 1939–1948.
16. Wu, Y.; Wang, J.; Liu, Z.; et al. Seasonal Nitrate Input Drives the Spatiotemporal Variability of Regional Surface Water-Groundwater Interactions, Nitrate Sources and Transformations. *J. Hydrol.* **2025**, *655*, 132973.
17. Zhao, Z.; Chen, Y.; Ye, C.; et al. Linkage between Nitrogen Loss, River Transport, Lake Accumulation and Water Quality Properties in Plain River Network Basin. *J. Environ. Sci.* **2025**, *157*, 65–76.
18. Dahan, O.; Babad, A.; Lazarovitch, N.; et al. Nitrate Leaching from Intensive Organic Farms to Groundwater. *Hydrol. Earth Syst. Sci.* **2014**, *18*, 333–341.
19. Han, Y.; Zhou, J.; Xia, F.; et al. Distribution of Nitrate Nitrogen and Oxygen Isotopes along the Hydrological Path in Alpine Forests. *China Environ. Sci.* **2025**, *45*, 935–942.
20. Xu, N.; Tan, G.; Wang, H.; et al. Effect of Biochar Additions to Soil on Nitrogen Leaching, Microbial Biomass and Bacterial Community Structure. *Eur. J. Soil Biol.* **2016**, *74*, 1–8.
21. Wickham, H. ggplot2. *WIREs Comput. Stat.* **2011**, *3*, 180–185.
22. Available online: https://CRAN.R-project.org/package=ggsignif (accessed on 12 October 2024).
23. Available online: https://cran.r-project.org/web/packages/agricolae/index.html (accessed on 18 April 2025).
24. Available online: https://cran.r-project.org/web/packages/Hmisc/index.html (accessed on 12 March 2025).
25. Available online: https://cran.r-project.org/web/packages/vegan/index.html (accessed on 22 January 2025).
26. Available online: https://github.com/DaliangNing/NST (accessed on 6 March 2025).
27. Bastian, M.; Heymann, S.; Jacomy, M. Gephi: An Open Source Software for Exploring and Manipulating Networks. In Proceedings of the International AAAI Conference on Web and Social Media, Media San Jose, CA, USA, 17–20 May 2009; pp. 361–362.
28. Wen, T.; Xie, P.; Yang, S.; et al. ggClusterNet: An R Package for Microbiome Network Analysis and Modularity-Based Multiple Network Layouts. *iMeta* **2022**, *1*, e32.
29. Huang, W.; Chen, X.; Wang, K.; et al. Comparison among the Microbial Communities in the Lake, Lake Wetland, and Estuary Sediments of a Plain River Network. *MicrobiologyOpen* **2019**, *8*, e00644.
30. Zhang, T.; Wang, W.; Leng, Y.; et al. Bacterial Diversity and Vertical Distribution Patterns in Sandy Sediments: A Study on the Bacterial Community Structure Based on Environmental Factors in Tributaries of the Yangtze River. *Microorganisms* **2024**, *12*, 1178.
31. Zhao, Z.; Zhao, R.; Qiu, X.; et al. Structural Diversity of Bacterial Communities and Its Relation to Environmental Factors in the Surface Sediments from Main Stream of Qingshui River. *Water* **2022**, *14*, 3356.
32. Pélabon, C.; Hilde, C.H.; Einum, S.; et al. On the Use of the Coefficient of Variation to Quantify and Compare Trait Variation. *Evol. Lett.* **2020**, *4*, 180–188.
33. Zhao, Y.-P. Characteristics and Influencing Factors of Soil Nitrogen-Cycling Microbial Communities under Different Land-Use Types. Ph.D. Thesis, Southwest University, Chongqing, China, 2024.
34. Sloan, W.T.; Lunn, M.; Woodcock, S.; et al. Quantifying the Roles of Immigration and Chance in Shaping Prokaryote Community Structure. *Environ. Microbiol.* **2006**, *8*, 732–740.
35. Chen, W.; Ren, K.; Isabwe, A.; et al. Stochastic Processes Shape Microeukaryotic Community Assembly in a Subtropical River across Wet and Dry Seasons. *Microbiome* **2019**, *7*, 138.
36. Ning, D.; Deng, Y.; Tiedje, J.M.; et al. A General Framework for Quantitatively Assessing Ecological Stochasticity. *Proc. Natl. Acad. Sci. USA* **2019**, *116*, 16892–16898.
37. Takeuchi, M.; Hamana, K.; Hiraishi, A. Proposal of the Genus *Sphingomonas* Sensu Stricto and Three New Genera, *Sphingobium*, *Novosphingobium* and *Sphingopyxis*, on the Basis of Phylogenetic and Chemotaxonomic Analyses. *Int. J. Syst. Evol. Microbiol.* **2001**, *51*, 1405–1417.
38. Liu, Y.; Pei, T.; Du, J.; et al. Comparative Genomic Analysis of the Genus *Novosphingobium* and the Description of Two Novel Species *Novosphingobium aerophilum* sp. nov. and *Novosphingobium jiangmenense* sp. nov. *Syst. Appl. Microbiol.* **2021**, *44*, 126202.
39. Li, Y.; Sun, Y.; Zhang, H.; et al. The Responses of Bacterial Community and N_2O Emission to Nitrogen Input in Lake Sediment: Estrogen as a Co-pollutant. *Environ. Res.* **2019**, *179*, 108769.
40. Huang, S.; Zhang, B.; Zhao, Z.; et al. Metagenomic Analysis Reveals the Responses of Microbial Communities and Nitrogen Metabolic Pathways to Polystyrene Micro (nano) Plastics in Activated Sludge Systems. *Water Res.* **2023**, *241*, 120161.
41. Reed, S.C.; Cleveland, C.C.; Townsend, A.R. Functional Ecology of Free-Living Nitrogen Fixation: A Contemporary Perspective. *Annu. Rev. Ecol. Evol. Syst.* **2011**, *42*, 489–512.
42. Ramond, J.-B.; Jordaan, K.; Díez, B.; et al. Microbial Biogeochemical Cycling of Nitrogen in Arid Ecosystems. *Microbiol. Mol. Biol. Rev.* **2022**, *86*, e00109-21.
43. Heylen, K.; Lebbe, L.; De Vos, P. *Acidovorax caeni* sp. nov., a Denitrifying Species with Genetically Diverse Isolates from Activated Sludge. *Int. J. Syst. Evol. Microbiol.* **2008**, *58*, 73–77.
44. Willems, A.; Gillis, M. Hydrogenophaga. In *Bergey's Manual of Systematics of Archaea and Bacteria*; Tindall, B.J., Ed.; Wiley: Hoboken, NJ, USA, 2015; pp. 1–15.
45. Kasalický, V.; Jezbera, J.; Hahn, M.W.; et al. The Diversity of the *Limnohabitans* Genus, an Important Group of Freshwater Bacterioplankton, by Characterization of 35 Isolated Strains. *PLoS ONE* **2013**, *8*, e58209.
46. Su, J.-F.; Zhang, K.; Huang, T.-L.; et al. Heterotrophic Nitrification and Aerobic Denitrification at Low Nutrient Conditions by a Newly Isolated Bacterium, *Acinetobacter* sp. SYF26. *Microbiology* **2015**, *161*, 829–837.
47. Giri, S.; Pati, B. A Comparative Study on Phyllosphere Nitrogen Fixation by Newly Isolated *Corynebacterium* sp. &

Flavobacterium sp. and Their Potentialities as Biofertilizer. *Acta Microbiol. Immunol. Hung.* **2004**, *51*, 47–56.
48. Lima, F.; Hadzibeganovic, T.; Stauffer, D. Evolution of Tag-Based Cooperation on Erdős–Rényi Random Graphs. *Int. J. Mod. Phys. C* **2014**, *25*, 1450006.
49. Guseva, K.; Darcy, S.; Simon, E.; et al. From Diversity to Complexity: Microbial Networks in Soils. *Soil Biol. Biochem.* **2022**, *169*, 108604.
50. Chen, Y.; Li, Y.; Qiu, T.; et al. High Nitrogen Fertilizer Input Enhanced the Microbial Network Complexity in the Paddy Soil. *Soil Ecol. Lett.* **2024**, *6*, 230205.
51. Banerjee, S.; Schlaeppi, K.; van der Heijden, M.G.; et al. Keystone Taxa as Drivers of Microbiome Structure and Functioning. *Nat. Rev. Microbiol.* **2018**, *16*, 567–576.
52. Spain, A.M.; Forsberg, C.W.; Krumholz, L.R.; et al. *Bergey's Manual of Systematics of Archaea and Bacteria*; Wiley: Hoboken, NJ, USA, 2015.
53. Anderson, C.R.; Condron, L.M.; Clough, T.J.; et al. Biochar Induced Soil Microbial Community Change: Implications for Biogeochemical Cycling of Carbon, Nitrogen and Phosphorus. *Pedobiologia* **2011**, *54*, 309–320.
54. Yu, M.; Su, W.Q.; Huang, L.; et al. Bacterial Community Structure and Putative Nitrogen-Cycling Functional Traits Along a Charosphere Gradient under Waterlogged Conditions. *Soil Biol. Biochem.* **2021**, *162*, 108420.
55. Qiu, L.; Fan, M.; Li, Y.; et al. Soil Phosphorus Drives Variation in Diazotrophic Communities in a Subtropical Nitrogen-Rich Forest. *For. Ecol. Manag.* **2023**, *544*, 121164**.**